RESEARCH ARTICLE

A Wideband Circularly Polarized CPW-Fed Printed Monopole X-Band Antenna for CubeSat Applications

MOHAMED EL HAMMOUMI[1], **FAISEL TUBBAL**[2,3], **(Senior Member, IEEE),**
NAJIBA EL AMRANI EL IDRISSI[1],
PANAGIOTIS IOANNIS THEOHARIS[2], **(Student Member, IEEE),**
SUHILA ABULGASEM[2], **(Student Member, IEEE), AND RAAD RAAD**[2], **(Member, IEEE)**

[1]Faculty of Sciences and Technologies, Sidi Mohamed Ben Abdellah University, Fes 30000, Morocco
[2]School of Electrical, Computer and Telecommunication Engineering, University of Wollongong, Wollongong, NSW 2500, Australia
[3]Technological Projects Department, Libyan Center for Remote Sensing and Space Science, Tripoli, Libya

Corresponding author: Faisel Tubbal (faisel@uow.edu.au)

ABSTRACT This paper presents a novel wideband circularly polarized CPW-fed printed monopole antenna for CubeSat applications. An AMC reflector with 5×5-unit cells is used to increase antenna gain. The overall size of the antenna is $0.48\lambda_0 \times 0.48\lambda_0 \times 0.042\lambda_0$ at the operating frequency of 8-GHz. The proposed printed monopole antenna provides a wide impedance bandwidth and a wide 3-dB axial ratio bandwidth. When comparing our proposed antenna to all designs, it is evident that the proposed printed monopole antenna offers several advantages. Firstly, it exhibits higher gain and a wider 3-dB axial ratio bandwidth (ARBW) while maintaining a smaller physical size. More specifically, the measured results show a wide -10 dB impedance bandwidth of 97.5% (6.1–13.9 GHz), and a wide measured 3-dB axial ratio bandwidth of 98.75% (5.1–13 GHz) and total measured gain of 7.3-dBi at 8 GHz.

I. INTRODUCTION

CubeSats have emerged as a notable class of miniaturized satellites, capturing considerable interest in the realm of space exploration and research. These satellites adhere to a standardized, cube-shaped design, measuring 10 centimeters per side (1U), and weighing a maximum of 1.33 kilograms [1], [2], [3]. CubeSats offer an accessible and cost-effective platform for conducting scientific experiments, showcasing technological advancements, and facilitating educational initiatives. Despite these challenges, ongoing research and advancements in technology continue to address and overcome the limitations of CubeSats. With their compact size and lower costs, CubeSats offer great potential for scientific exploration, technology development, and educational initiatives, paving the way for innovative and accessible space missions [4]. Antennas play a critical role in CubeSat

missions as they provide crucial communication capabilities between the satellite and ground stations. Antennas designed for CubeSats must address several challenges due to the satellite's small form factor and limited power and weight restrictions. The antenna must be compact, lightweight, and efficient while maintaining reliable and robust communication links.

In modern wireless communication, there is a necessity to use antennas that generate Circular Polarization (CP) radiation with high data rate and high gain, especially in the CubeSat and terrestrial point-to-point communication systems [5], [6]. This is because CP allows the establishment of a communication link between the transmitting and receiving antennas, even if their polarization planes are not perfectly aligned. This ensures more stable and consistent communication links between satellites, spacecraft, and ground stations [7]. Furthermore, CP radiation alleviates the Faraday rotation effect which otherwise causes the linear vector to rotate as a consequence of its interaction with the

The associate editor coordinating the review of this manuscript and approving it for publication was Shah Nawaz Burokur.

static magnetic field [8]. Additionally, among the prominent advantages of CP are the mitigation of fading effects and multipath rejection that cause interference in the linear polarization [9].

There are two main approaches for generating CP radiation which include the use of both the single-fed CP technique and the dual-fed CP technique [10], [11]. The main advantages of the single fed are its low profile, simplicity, low fabrication cost, and compact size [12]. However, its main limitations are the resulting narrow 3dB Axial Ratio (AR) and −10dB impedance bandwidths (IBW). On the other hand, the dual-fed CP approach offers a broadband 3dB ARBW and a wide IBW. However, it occupies a larger space and necessitates an external hybrid polarizer, which poses challenges in integrating it into modern compact devices and adds complexity to the overall design.

From the two aforementioned method for CP generation, the single-fed CP technique is the most suitable for CubeSats due to its compact size. Single fed CP antennas can be designed using either printed slot and monopole antennas with biplanar or uniplanar structures [6]. The authors of [6], present a comprehensive comparative study between printed slot and monopole antenna structures based on various works reported in the literature. The study concludes that printed monopole antennas (Coplanar Waveguide (CPW-fed)) exhibit broader ARBW and IBW that exceed 100%. They also demonstrate high trade-off values in terms of ARBW/size and IBW/size, while maintaining a compact size.

Accordingly, the authors of [13], presented a broadband C-shaped CP monopole antenna that provides a 3dB ARBW of 65.2%, an IBW of 87.7%, and a total gain of 3.5 dBi at 6 GHz. To achieve a broad CP, the authors placed a rectangular open-loop that was coupled with the Monopole and they connected a rectangular stub with the ground. Another C-shaped CP Monopole antenna is proposed by the authors of [14]. To achieve a wide IBW and ARBW, they cut the corner of the combined C-shaped patch and added triangular stubs on the ground plane. They reported 95.2% IBW and 96.8% 3dB ARBW and a peak gain of 3dBi at 4 GHz. However, the primary drawback of this proposed antenna is its low gain. In [15], Ellis et al. proposed an Asymmetric CP open-slot antenna for WLAN, ISM, WiMAX, and C-band applications. The main idea was to feed the open asymmetric wide circular open slot by an offset feedline with an attached short stub. The proposed antenna provides a wide CP bandwidth of 61% and a total gain of 4 dBic at 3.5 GHz. In addition, a CP square slot antenna is presented in [16], where the authors modified the conventional square-slot-based ground to the CP bandwidth. They reported a 2dB ARBW of 54.2%, a 10-dB IBW of 92.7%, and a total gain of 4.5 dBic at 7.8 GHz. Another CP square slot antenna is proposed in [17]. The authors used the CPW-fed technique to feed the proposed square slot antenna with a grounded L-strip and I-shaped radiator. The proposed antenna provides a 3dB ARBW of 33.96%, an IBW of 116%, and a peak gain of 5.92 dBi at 11 GHz.

The main limitation of all the above-mentioned designs is their low gains. One solution to improve the antenna gain is to use an Artificial Magnetic Conductor (AMC) as reflector redirect the back radiation forward and hence increase the antenna gain [18], [19], [20], [21], [22]. The AMC artificial characteristic is the in-phase reflection (0° phase) at a distance close to the radiating element which makes it different from the Perfect Electric Conductor (PEC) reflector. The latter needs a minimum distance of $\lambda/4$ to avoid destructive interference. However, due to its in-phase reflection characteristics, the AMC reflector can effectively serve the same purpose as a PEC, but at a close distance to the radiating element. This enables the maintenance of a low-profile structure for both the antenna and the AMC reflector [23]. Finally, AMC can also be considered as metamaterials that consist of periodic metallic structures. As mentioned in [24] it is important to be able to visualize and study the edge waves that exist between the interface of air and AMC surfaces.

In this paper, a circular polarized CPW-fed printed monopole antenna with AMC that operates in the X-band is presented. Operating in the X-band frequency range for CubeSat antennas provides number of advantages, such as miniaturization of the antenna to meet size and weight restrictions, and higher data rates [25]. Both the monopole and the ground planes are etched onto an FR4 dielectric substrate. To achieve CP, the asymmetric ground planes are adopted and a proper triangular cut in the upper edge of the right ground plane is made as shown in Fig. 1. Moreover, the AMC metasurface is used as a reflector to redirect the back lobe radiation forwarded and hence enhance the proposed antenna's gain. The antenna is measured and fabricated. The proposed antenna has a small size, low profile, and simple feeding structure. The discussed results and design procedure are presented in the following sections.

II. DESIGN PROCESS OF PROPOSED ANTENNA

This section presents the structural evolution process of the proposed PMA with AMC. For our proposed design, we have considered the techniques presented in [6], [26], and [27] as the design guidelines to the start of our design. Moreover, based on the slot structure outlined in [27], we introduced the asymmetrical ground plane characterized by varying the heights. This leads to the excitation of the CP operation while simultaneously achieving the desired impedance matching.

A. PRINTED MONOPOLE ANTENNA DESIGN

Fig. 1 shows the geometry of the proposed CPW-fed printed monopole antenna. The antenna operates at a resonant X-band frequency of 8 GHz and consists of a microstrip CPW-fed printed monopole wherein the monopole and the ground planes are on the same side (top side). The ground planes (in orange color) are separated by the same optimized distance gap g = 0.25mm from the monopole. The optimum dimensions of the three metallic (PEC) parts (in orange color) namely the monopole, the left and the right ground planes

as well as the substrate dimensions are listed in Table 1. The antenna is placed above AMC (thickness of its dielectric substrate (in green color) is 0.8mm) at height $h_1 = 4.8$ mm (0.128λ) and is fed by a 50 Ω CPW line. The characteristic impedance of CPW feed is not inherently set at 50 Ω. It can vary based on the design parameters of the CPW structure, such as the dimensions of the signal trace (i.e., W_m and L_m), the distance gap between the signal trace and the ground planes (i.e., g) and the dielectric constant of the substrate material [28], [29]. The AMC reflector is a lattice of 5×5-unit cell with periodicity of p=6.2mm (0.165λ). The optimum value of arc-truncation radius is 1.9mm. The upper substrate (in Agua colour used is FR4 with a dielectric constant of 4.4, a loss tangent of 0.02, and a thickness of h=1.6mm. The size of the antenna is $0.48\lambda_0 \times 0.48\lambda_0 \times 0.042\lambda_0$ at an operating frequency of 8 GHz. The photograph of the fabricated prototype is shown in Fig. 2.

To provide insight into the development of the final design and to show how the final printed monopole antenna design is obtained, a comparative analysis is carried out among three intermediate antennas (Ants. 1-3) aa shown in Fig. 7. This evaluation is undertaken to examine and contrast the performance characteristics of each antenna relative to one another. The generation of CP radiation is obtained by making a triangular cut at the up edge of the right ground plane beside the well-known impact of the asymmetric ground planes of the CPW-fed PMA as shown in Fig.1 and 2. The optimum height h_{tr} of this equilateral triangle (the cut part) is 5.25 mm. Fig. 3 depicts the surface current distribution of Ant.1 (symmetric ground planes with no cut), see Fig. 7(a). We can see that the surface current vectors in both ground planes are approximately in the same horizontal direction but in opposite directions, which means that the horizontal component of the electric field is reduced. This is explained by the fact that the surface current vectors in each ground plane cancel each other. As a result, the antenna becomes vertically linearly polarized.

Fig. 4, shows the surface current distribution for Ant. 3 (see Fig. 7(c) at four phases 0°, 90°, 180°, and 270°. We see that the implementation of asymmetric ground planes and the incorporation of triangular cuts led to the achievement of equal horizontal and vertical components, along with the attainment of phase quadrature. The arrow at phi = 0° (left) is the reference and as the surface current arrows are in the counterclockwise direction for the four-phase times, then the CP type for this proposed antenna is RHCP in the boresight (+z) direction and LHCP in the backside (–z) direction regarding the bidirectional radiation of the CPW-fed PMA. The impact of the triangular cut is evident, as observed in the considerable reduction of AR values within the targeted frequency range. This effect can be further explained by considering the perturbation it introduces in the surface current. This perturbation is causing the horizontal electric field component to equate its vertical counterpart while maintaining a phase quadrature relationship. It is important to note that this analysis is conducted in reference to the

unchanged configuration of the CPW-fed planar monopole antenna (refer to Ant.1), depicted in Fig 3.
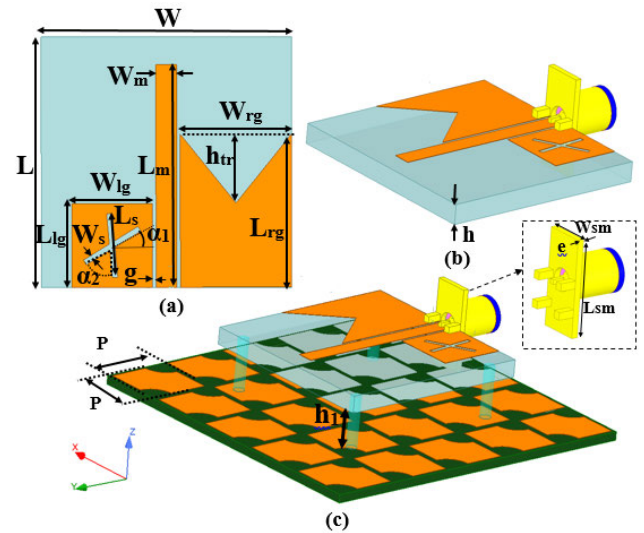

FIGURE 1. Configuration of CPW-fed PMA (a) geometry PMA, (b) PMA on substrate, and (c) the model of PMA with AMC in HFSS.
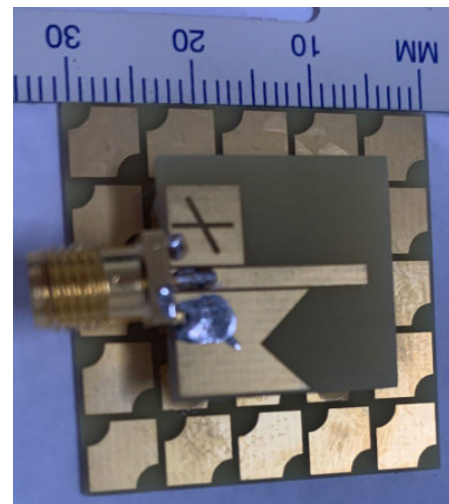

FIGURE 2. Photograph of antenna prototype.

B. AMC REFLECTOR DESIGN

The AMC surfaces are class of a metasurfaces that have an engineered (artificial) behavior which act as the in-phase reflector similar to a Perfect Magnetic Conductor (PMC) [30]. The latter is characterized by its high impedance surface, where the tangential component of the magnetic field is eliminated, resulting in a surface current density of zero. As a result, incoming electromagnetic waves are reflected with a 0° phase shift, promoting constructive interference. These properties open up possibilities for the development of more compact antennas with reduced mutual coupling and improved front-to-back ratio (FBR). For instance, incorporating an AMC metasurface as a reflector behind a
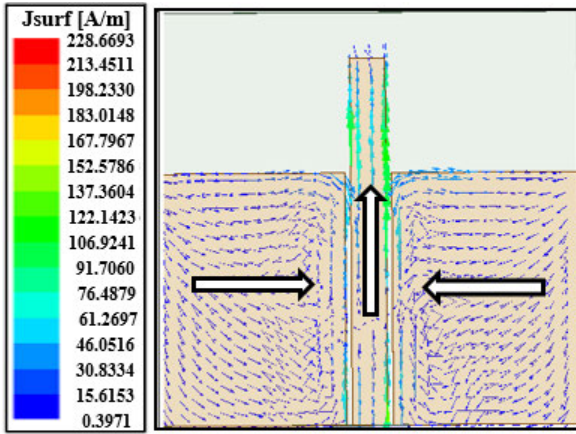
FIGURE 3. The surface current vector on monopole and ground planes.
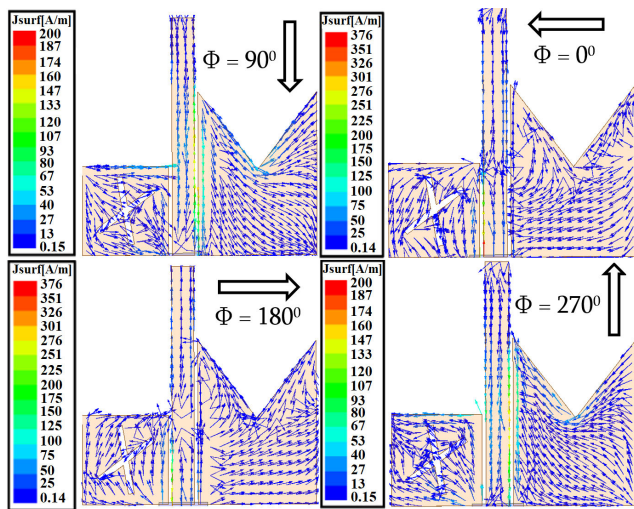

FIGURE 4. The surface current distribution at phases: 0°, 90°, 180° and 270°.

radiating element allows for a smaller distance between them, less than $\lambda/4$, leading to a low-profile structure.

To achieve the artificial characteristic of the AMC reflector, our initial approach involved designing a unit cell with a simple uniplanar metallic square shape, departing from the mushroom or biplanar forms previously reported [31]. This choice was preferred due to its ease of integration with electronic components, eliminating the need for a ground plane (which could result in cancelling the current in the patch), and lower fabrication costs [32]. The reflection response in terms of phase and amplitude versus frequency of this unit cell was obtained through the following steps:

1) The unit cell is designed to exhibit an in-phase reflection property, ensuring a 0° phase shift that guarantees constructive interference. This property holds true for a plane wave with normal incidence across a broad bandwidth. At the center frequency of 8 GHz, the reflection phase of the unit cell ranges between −90° and +90°.

2) The unit cell is modeled using the HFSS software [33], employing a Finite Element Method (FEM) based on the Floquet theory. This approach enables the periodic structure to exhibit AMC behavior within the desired frequency range. The full wave analysis provided by the HFSS software ensures accurate characterization of the unit cell's electromagnetic properties.

Fig. 5 illustrates the implementation of an infinite model, achieved by applying Floquet boundary conditions (Floquet port) at the top of the unit cell, along with primary (master) and secondary (slave) boundaries on the side walls. The proposed unit cell consists of a square patch printed onto an FR4 dielectric substrate. As shown in Fig. 5 and Table 1, its geometrical parameters are the width of the patch **Wp**, the periodicity **P** and the thickness of the substrate **hu**. The distance **d** between the top side of the patch and the Floquet port excitation is taking to be $\lambda/4$. The selection of an appropriate distance between the port and the surface of patch requires careful consideration. If this distance is too small, the near fields generated by the scatterer interact with the ports, leading to numerical inaccuracies. Conversely, if the ports are positioned too far, the computational time becomes unreasonably prolonged. The optimal distance ensures that the evanescent near fields have attenuated to an insignificant level. The unit cell itself consists of a square patch with optimized dimensions of $5.6 \times 5.6 \times 0.035 \text{mm}^3$. This patch is etched onto an FR4 dielectric substrate measuring $6.2 \times 6.2 \times 1.6 \text{mm}^3$. Moreover, by exploring different sizes of the unit cell, we were able to identify the optimal configuration that yields a desirable reflection response in terms of phase and magnitude at the operating frequency of 8 GHz, as depicted in Fig. 6. This configuration presents an in-phase reflection with a wide fractional ±90° bandwidth of 25.25% (7.05-9.07GHz) around the center frequency of 8 GHz. The dip in the magnitude of the reflection confection at 8 GHz is due to the losses in the dielectric material and the AMC conductor. However, the obtained result is good as it shows a good zero reflection phase at the resonance frequency of 8 GHz.
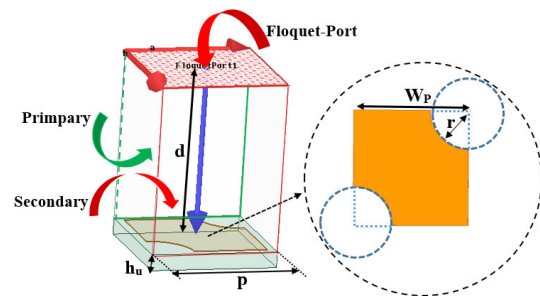

FIGURE 5. 3D view of the unit cell.

III. PARAMETRIC STUDY

In this section, we present a range of parametric analyses that were carried out using HFSS. We focus on achieving an optimal reflection coefficient, AR, and gain specifically at the
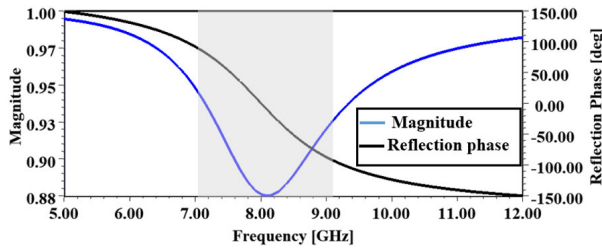
FIGURE 6. Phase and magnitude reflection of MLPF unit cell.

operating frequency of 8 GHz. To accomplish this, we utilized the Quasi-Newton method within the HFSS software for parametric optimization. The Quasi-Newton method, a computer-aided finite element method-based optimization tool, was employed to attain the best possible results. This optimization method functions by seeking to uncover the lowest or highest point of a cost function, while making adjustments to the variables within specified constraints. for example for variable "g", the decision variable is the gap distance "g" between ground planes, which spans from 0.1 mm (minimum) to 0.6 mm (maximum). The objective revolves around achieving a minimal reflection coefficient (a design parameter) at the specified operational frequency of 8 GHz (a constraint). To fulfill this, the Quasi-Newton method endeavors to decrease the reflection coefficient's value (S11) through successive iterations. These iterations entail varying the gap distance 100 times, progressing from 0.1 mm to 0.6 mm. The step sizes utilized are 0.013 mm for the minimum and 0.13 mm for the maximum values. The optimal parameters of the proposed antenna are listed in Table 1.

A. DESIGN OF THE PMA STRUCTURE

Fig. 7 illustrates the design process of the proposed antenna, commencing from Ant.1 and concluding at Ant.3. The evaluation process of the proposed antenna is as follows:

1) As depicted in Figure 7(a), **Ant.1** is the initial stage that involved the design of a printed monopole uniplanar antenna with symmetric ground planes that operates at 8 GHz (**Ant.1**). As shown in Fig. 8 and 9, the initial antenna design exhibits a relatively narrow fractional −10 impedance bandwidth of 12.8% (8.1-9.2 GHz) and maintained a linear polarization characteristic, respectively. This was evident from the high values of AR, exceeding 3dB, within the frequency range of interest, as illustrated in Fig. 9.

2) To improve the IBW and AR, we implemented asymmetric ground planes and introduced an X-shaped slot through etching on the left ground plane, as illustrated in Fig. 7(b). Ant.2 demonstrates a performance improvement as compared to Ant. 1. It provides IBW of 40.14% (5.6-8.45 GHz) centred around 7.1 GHz, with a reflection coefficient of −15 dB, see Fig. 8. In addition, it achieves an AR of approximately 9 dB at 7.1 GHz. This is an important improvement regarding the generation of CP radiation as compared to Ant.1.

TABLE 1. Optimal parameters of the proposed antenna.

	Variable	Dimensions (mm)	Material
Radiator	W_m	1.5	Copper
	L_m	16	
	g	0.25	
Substrate	W	18	FR4
	L	18	
	h	1.6	
Ground	(L_{lg}, W_{lg})	(6,5.8)	Copper
	(L_{rg}, W_{rg})	(11.8)	
	h_{tr}	4.15	
	(L_s, W_s)	(4.608, 0.4)	
	α_1	35°	
	α_2	45°	
SMA	(L_{sm}, W_{sm})	(7.62,3)	PEC
	e	0.5	
Unit cell	Wp	5.6	PEC
	r	1.9	
	h_u	1.6	FR4
	P	6.2	

3) The final design, as depicted in Fig 7(c), incorporates a triangular cut made at the upper edge of the right ground plane in Ant.3. This modification has resulted in a significant enhancement in antenna performance as well as enabling it to achieve CP radiation. As shown in Fig. 8, successfully achieves an exceptionally wide IBW of 107.5% (4.5-13.1 GHz), with a small reflection coefficient of −33 dB at 8 GHz. Moreover, as shown in Fig. 9, the final design (e.g., Ant.3) exhibits a CP radiation pattern, offering a wide 3dB ARBW of 73.75% (7.35-13.25 GHz) with an AR of 0.3 dB at 8 GHz. Notably, there is a significant overlap between the ARBW and the IBW, indicating a favourable performance characteristic of the antenna. The introduction of asymmetric ground planes perturbs the surface current, effectively enhancing the strength of the horizontal electric field component. In that way CP radiation is achieved, while the triangular cut leads to a substantial reduction in AR values across the frequency range of interest. This reduction is explained by optimally positioning the triangular cut heights (h_{tr}) as illustrated in Fig. 10 and Fig. 11, wherein the perturbation of the surface current proves adequate to establish equal electric field components, each in phase quadrature, as portrayed in Fig. 4.
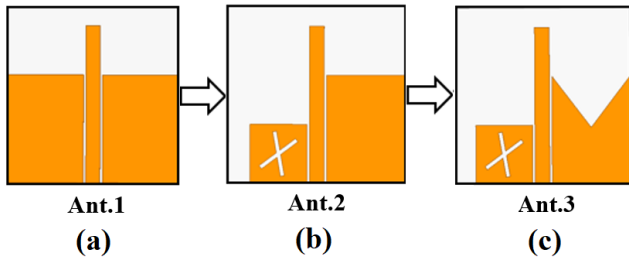
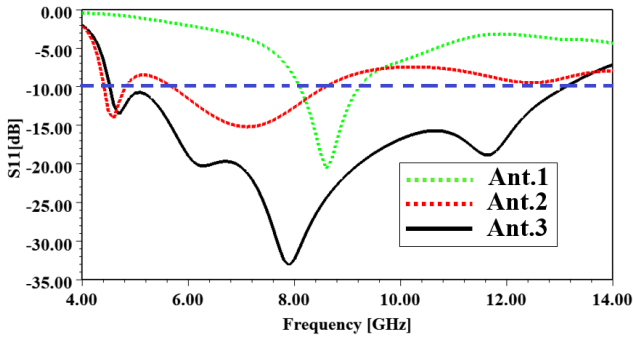**FIGURE 7.** Design process of proposed printed monopole antenna.

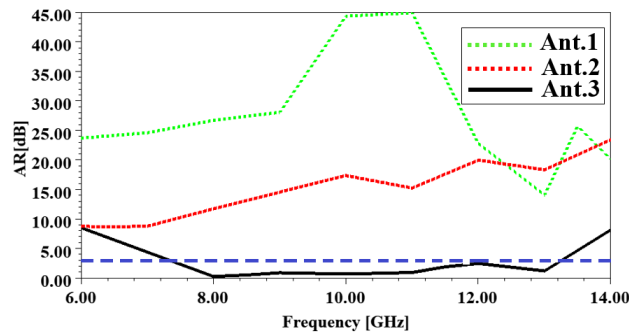**FIGURE 8.** Simulated reflection coefficient against frequency.

FIGURE 9. Simulated AR against frequency at $\theta = 0°$, $\Phi = 0$.

B. EFFECT OF h_{tr}

Fig. 10 illustrates the reflection coefficient for different triangular cut heights (h_{tr}): 0 mm, 2.625mm, and 5.25mm, while keeping all other parameters constant. We see that the height of the triangular cut has a significant effect on the reflection coefficient (S11) and the -10dB IBW, whereas its impact on the operating frequency is comparatively minimal. When the height h_{tr} increases (e.g., exceeds 2.6) the reflection coefficient decreases and the IBW improves. The optimal value of h_{tr} is determined to be 5.25mm, which results in the lowest reflection coefficient of -33 dB at 8 GHz, as well as a wide IBW of 107.5% ranging from 4.5 GHz to 13.1 GHz. Furthermore, the impact of h_{tr} on the AR is demonstrated in Fig. 11. The graph indicates a decrease in the AR as h_{tr} value increases, particularly when it exceeds 2.625mm. The most favorable htr value is determined to be 5.25mm, resulting in a broad CP AR of 73.75% with a low AR of 0.3 dB at operating frequency of 8 GHz.
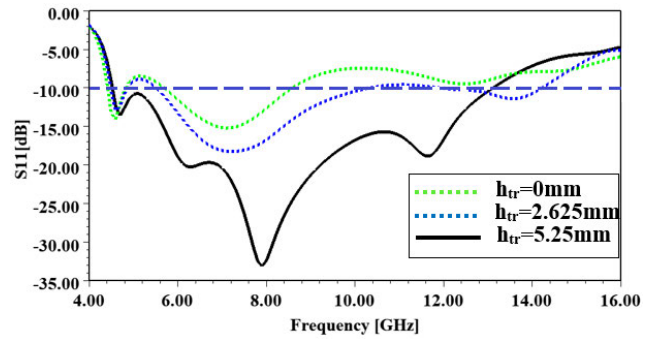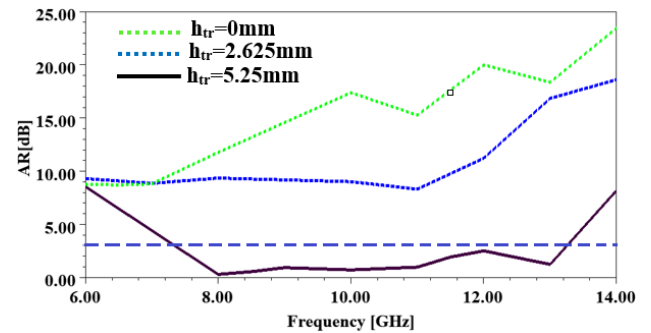

FIGURE 10. The effect of h_{tr} on S11 without AMC.

FIGURE 11. The effect of h_{tr} on AR without AMC at $\theta = 0°$, $\Phi = 0$.

C. EFFECT OF L_m

Fig. 12 and Fig. 13 depict the S11 and AR, respectively, for various monopole lengths (L_m) of 15mm, 15.5mm, and 16.0mm. All other parameters are held constant. Comparing the results at 8 GHz, it is observed that monopole lengths of 15.5mm and 16mm yield lower reflection coefficients and AR as compared to the length of 16.0mm. The optimal monopole length that achieves a wide 3dB ARBW (e.g., 73.75%) and wide IBW (107.5%) is determined to be the best choice.
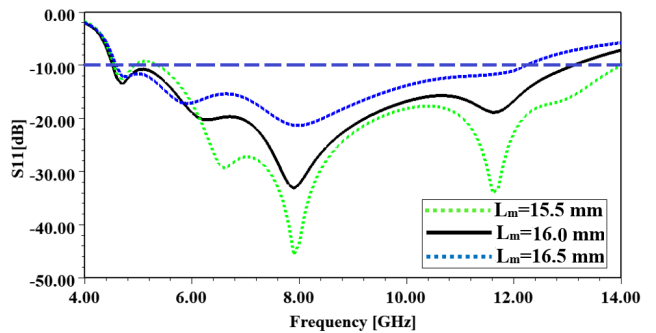

FIGURE 12. The effect of Lm on S11 without AMC.

D. EFFECT OF AMC

In this section, we now study the effect of the AMC on the proposed antenna performance (e.g., gain, S11 and AR). Fig. 14 presents the total gain of the proposed CPW-fed printed monopole antenna, comparing the scenarios with and without the utilization of the AMC. It is evident that
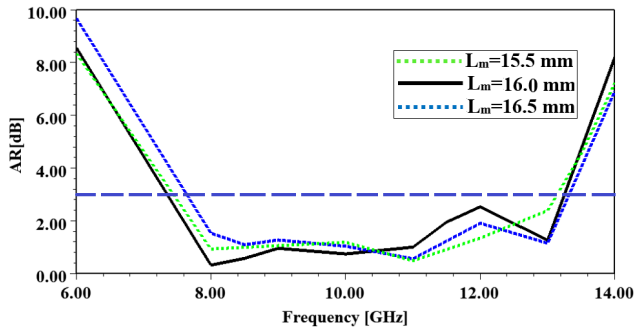
FIGURE 13. The effect of Lm on AR without AMC at $\theta = 0°$, $\Phi = 0$.

incorporating the AMC leads to a significant redirection of the back lobe, resulting in a remarkable increase in the antenna's gain. Specifically, the antenna's gain rises from 2.4 dBi to 7.4 dBi, showcasing a substantial improvement achieved using the AMC.

Fig. 15 and 16 illustrate the reflection coefficient and axial ratio of the proposed antenna respectively, both with and without the AMC. With the incorporation of the AMC, there is an increase in the S11 from -33 dB to -23 dB while maintaining the operating frequency at 8 GHz. Although, even with the AMC, the antenna still maintains a wide IBW of 97.5% (6.40-14.2 GHz). Additionally, it exhibits a wide ARBW of 91.37% (5.59-12.90 GHz).
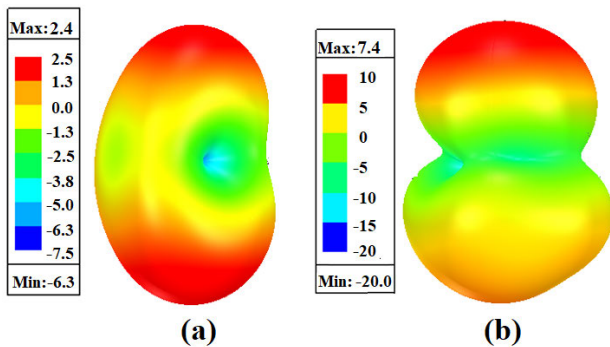

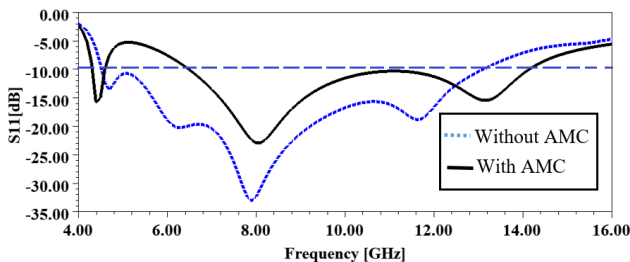**FIGURE 14.** The total gain of PMA (a) without AMC, and (b) with AMC.

FIGURE 15. Simulated S11 against frequency.

IV. EXPERIMENTS AND COMPARISONS
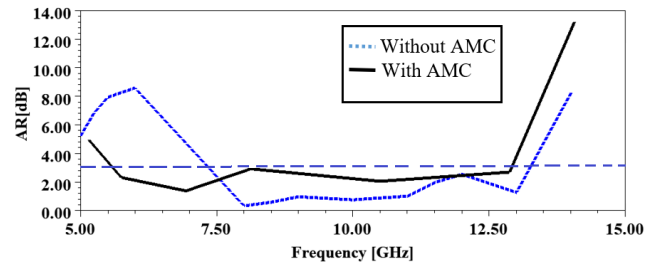In order to validate the accuracy of the simulation results, a prototype of the proposed CP printed monopole antenna

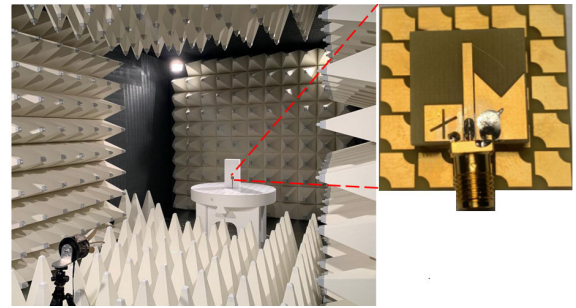**FIGURE 16.** Simulated AR against frequency at $\theta = 0°$, $\Phi = 0$.

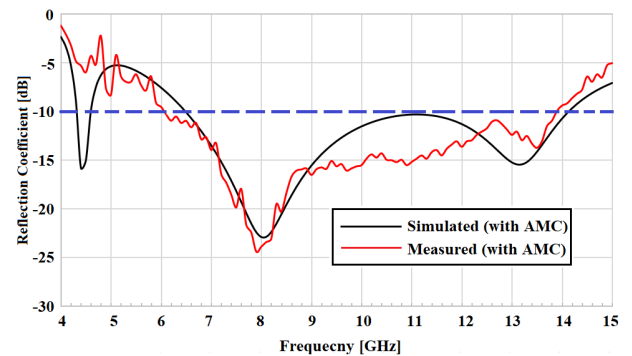**FIGURE 17.** Antenna undergoing measurement inside anechoic chamber.
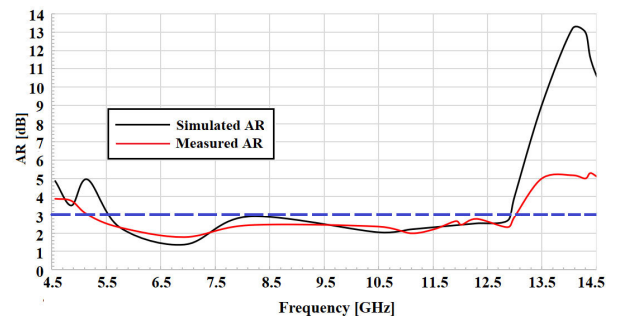

FIGURE 18. Simulated and measured S11 with AMC.

FIGURE 19. Simulated and measured AR at $\theta = 0°$, $\Phi = 0$.

was manufactured and measured in an anechoic chamber, as illustrated in Fig. 17. We adhered to the test procedures outlined by IEEE standards to evaluate the performance of the proposed antenna [34]. Measurement of the fabricated antenna's reflection coefficients was carried out employing Keysight's E5063A Vector Network Analyzer (VNA) and the corresponding calibration kit. The assessment
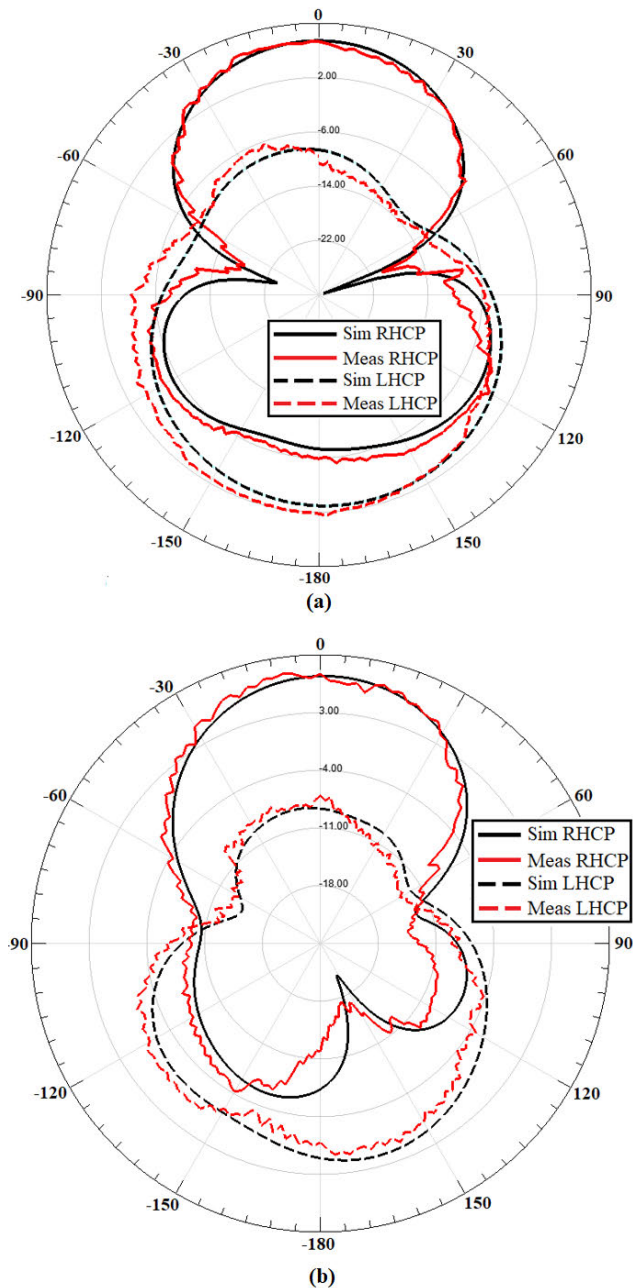
FIGURE 20. RHCP and LHCP radiation patterns of the proposed antenna for (a) Phi = 0 and (b) Phi = 90 at 8 GHz.

FIGURE 21. RHCP and LHCP radiation patterns of the proposed antenna for (a) Phi = 0 and (b) Phi = 90 at 10 GHz.

of the antenna's radiation pattern was executed within a far-field anechoic chamber situated at the University of Wollongong's laboratory. This controlled environment effectively eliminates external interference and reduces undesirable reflections, thereby ensuring the measurement conditions closely approximate the reflectionless simulation environment in HFSS. The measured and simulated S11 and AR of the proposed printed monopole antenna are presented in Fig. 18 and 19, respectively. The antenna exhibits a wide measured −10 dB impedance bandwidth (IBW) 97.5% ranging 6.1 GHz to 13.9 GHz, along with a wide measured
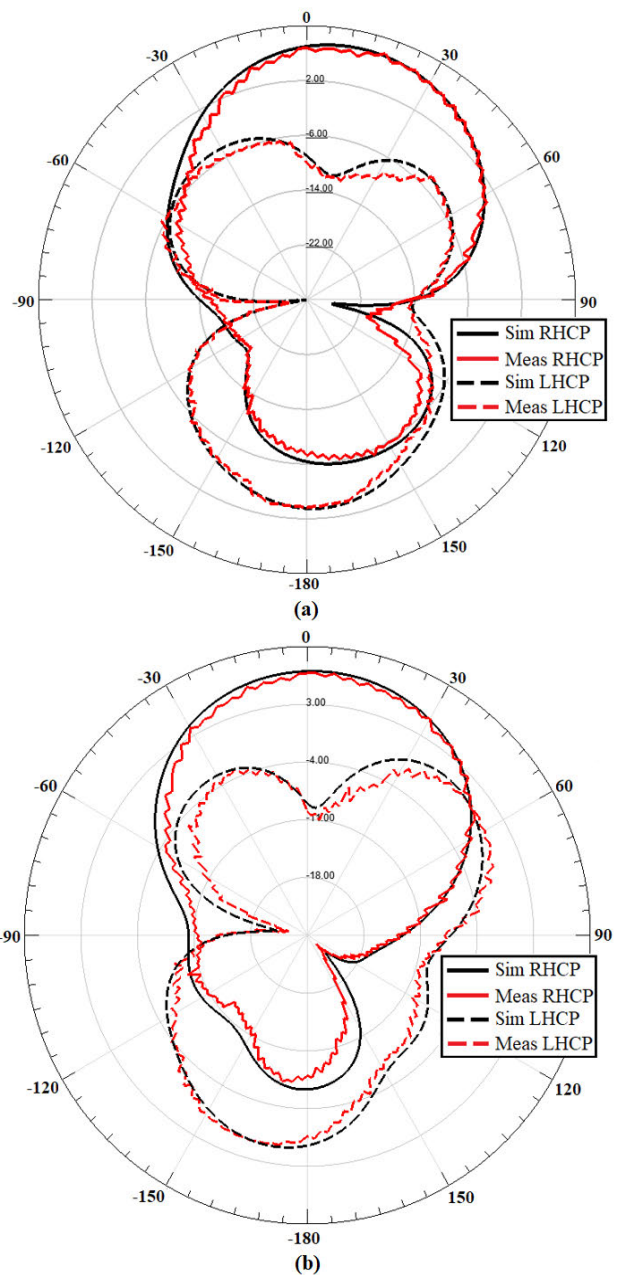
3 dB ARBW of 98.75% within the frequency range of 5.1-13 GHz. At 8 GHz, the measured S11 is −23.92 dB, and AR is 2.4 dB.

Fig. 20, 21 and 22 show the simulated and measured radiation patterns (e.g., LHCP and RHCP) at three different frequencies of 8, 10 and 12 GH for phi = 0^0 and phi = 90^0 respectively. A satisfactory agreement is observed between the measured and simulated radiation patterns. We can conclude that the proposed antenna achieves good performance of RHCP radiation in the +z-direction. Moreover, Fig. 20 shows that in both the E-plane and H-planes, the isolation between cross-polarization and co-polarization is less than -
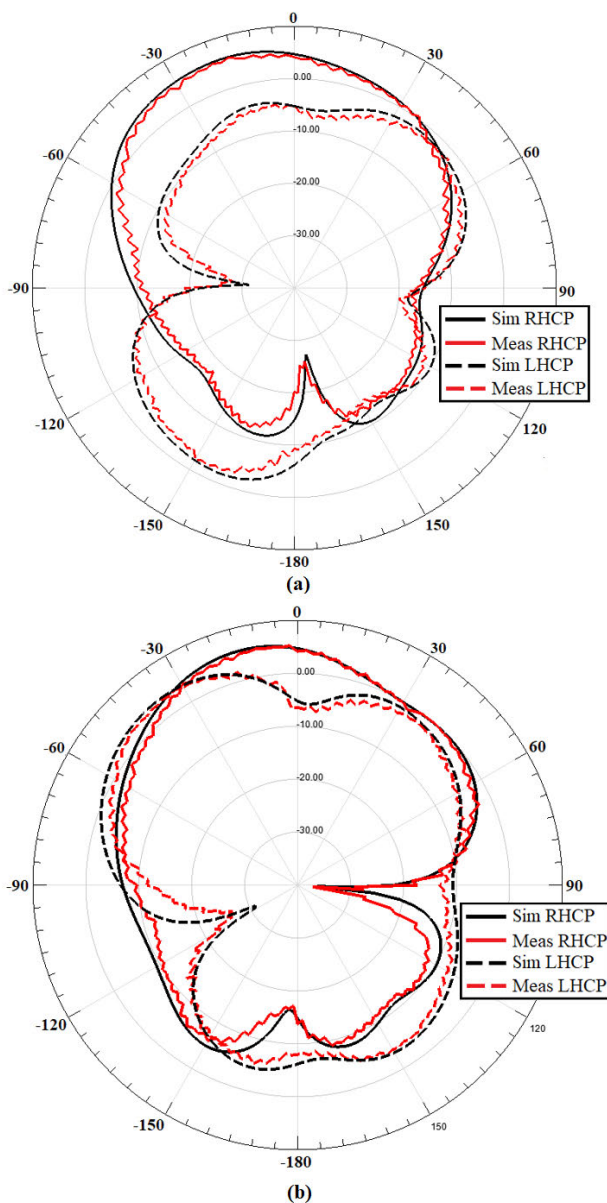
FIGURE 22. RHCP and LHCP radiation patterns of the proposed antenna for (a) Phi = 0 and (b) Phi = 90 at 10 GHz.

15 dB at the broadside direction. In addition, the measured and simulated broadside gain versus frequency is depicted in Fig. 23. We can see that the simulation agrees well with the measured results across the band (e.g., 7 – 13 GHz) with a small discrepancy of less than 1 dB. This discrepancy is due to fabrication errors. The measured gain at 8 GHz is 7.3 dBi.

Lastly, the performance of the proposed printed monopole antenna is compared with other existing antenna designs referenced in Table 2. The comparison encompasses aspects such as impedance and axial ratio bandwidths, gain, and size. Compared to all designs presented in Table 2, the proposed printed monopole antenna printed monopole antenna provides higher gain, wider 3dB ARBW and has smaller size.
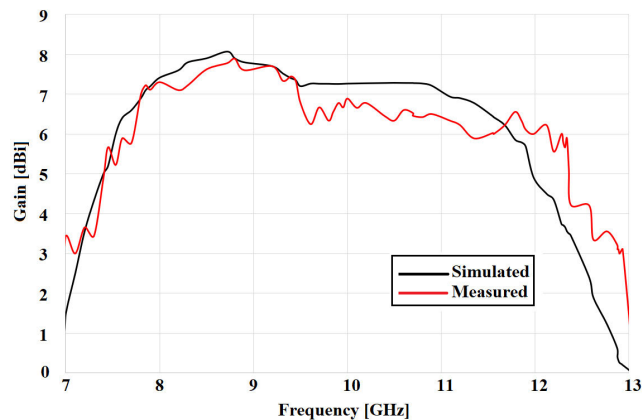

FIGURE 23. Simulated and measured gain of the proposed antenna.

In terms of −10 dB IBW, the proposed antenna provide wider bandwidth as compared to [13], [14], and [16].

TABLE 2. Comparison between our CPW-fed PMA results and other recent results in the literature.

Ref	Gain (dBi)	-10dB IBW (%)	3dB ARBW (%)	Size ($\lambda_0 \times \lambda_0 \lambda_0$)	Substrate
[13]	3.5	87.7	65.2	0.6×0.63×0.025	FR4
[14]	3	95.2	96.8	0.7×0.7×0.028	FR4
[15]	4	125	61	0.71×71×0.045	FR4
[16]	4.5	92.7	54.2	0.8×0.8×0.016	FR4
[17]	5.92	116	33.96	0.53×0.53×0.04	Rogers RO3000
This work	**7.3**	**97.5**	**98.75**	**0.48×0.48×0.042**	**FR4**

V. CONCLUSION

In this paper, a wideband CP printed dipole antenna using AMC is proposed for CubeSat applications. The gain of the proposed antenna is improved by placing AMC at the back of the antennas. In order to attain CP, the design incorporates asymmetric ground planes and introduces a triangular cut at the upper edge of the right ground plane. Compared to all antenna design presented in Table 2, our proposed printed monopole antenna demonstrates a higher gain and a wider 3dB ARBW while occupying a smaller physical footprint. Furthermore, in relation to the −10 dB IBW, the proposed antenna offers a broader bandwidth designs as compared to the designs of [13], [14], and [16].The antenna provides a wide −10 dB IBW and 3dB ARBW of 97.5% and 98.75 respectively. It achieves a measured total gain of 7.3dBi at 8 GHz (e.g., X-band) and has a total size of $0.48\lambda_0 \times 0.48\lambda_0 \times 0.042\lambda_0$.

REFERENCES

[1] S. Gao, K. Clark, M. Unwin, J. Zackrisson, W. A. Shiroma, J. M. Akagi, K. Maynard, P. Garner, L. Boccia, G. Amendola, G. Massa, C. Underwood, M. Brenchley, M. Pointer, and M. N. Sweeting, "Antennas for modern small satellites," *IEEE Antennas Propag. Mag.*, vol. 51, no. 4, pp. 40–56, Aug. 2009.

[2] S. Abulgasem, F. Tubbal, R. Raad, P. I. Theoharis, S. Lu, and S. Iranmanesh, "Antenna designs for CubeSats: A review," *IEEE Access*, vol. 9, pp. 45289–45324, 2021.

[3] F. E. Tubbal, R. Raad, and K.-W. Chin, "A survey and study of planar antennas for pico-satellites," *IEEE Access*, vol. 3, pp. 2590–2612, 2015.

[4] N. Chahat, *CubeSat Antenna Design*. Dec. 2020. [Online]. Available: https://onlinelibrary.wiley.com/doi/book/10.1002/9781119692720, doi: 10.1002/9781119692720.

[5] S. S. Gao, Q. Luo, and F. Zhu, *Circularly Polarized Antennas*. Nov. 2014. [Online]. Available: https://onlinelibrary.wiley.com/doi/book/10.1002/9781118790526, doi: 10.1002/9781118790526.

[6] U. Banerjee, A. Karmakar, and A. Saha, "Circularly polarized antennas: An evident advancement in modern wireless communications," in *Innovative Smart Materials Used in Wireless Communication Technology*. Hershey, PA, USA: IGI Global, 2023, pp. 176–200.

[7] B. Yen Toh, R. Cahill, and V. F. Fusco, "Understanding and measuring circular polarization," *IEEE Trans. Educ.*, vol. 46, no. 3, pp. 313–318, Aug. 2003.

[8] C. A. Balanis, *Antenna Theory: Analysis and Design*, 3rd ed. Hoboken, NJ, USA: Wiley, 2016.

[9] A. J. A. Al-Gburi, Z. Zakaria, H. Alsariera, M. F. Akbar, I. M. Ibrahim, K. S. Ahmad, S. Ahmad, and S. S. Al-Bawri, "Broadband circular polarised printed antennas for indoor wireless communication systems: A comprehensive review," *Micromachines*, vol. 13, no. 7, p. 1048, Jun. 2022.

[10] Q.-S. Wu, X. Zhang, and L. Zhu, "A feeding technique for wideband CP patch antenna based on 90° phase difference between tapped line and parallel coupled line," *IEEE Antennas Wireless Propag. Lett.*, vol. 18, no. 7, pp. 1468–1471, Jul. 2019.

[11] W. Yang, J. Zhou, Z. Yu, and L. Li, "Single-fed low profile broadband circularly polarized stacked patch antenna," *IEEE Trans. Antennas Propag.*, vol. 62, no. 10, pp. 5406–5410, Oct. 2014.

[12] Z. Wang, S. Fang, S. Fu, and S. Jia, "Single-fed broadband circularly polarized stacked patch antenna with horizontally meandered strip for universal UHF RFID applications," *IEEE Trans. Microw. Theory Techn.*, vol. 59, no. 4, pp. 1066–1073, Apr. 2011.

[13] K. Ding, C. Gao, T. Yu, and D. Qu, "Broadband C-shaped circularly polarized monopole antenna," *IEEE Trans. Antennas Propag.*, vol. 63, no. 2, pp. 785–790, Feb. 2015.

[14] Z. Y. Li, X. S. Zhu, C. Y. Yin, and Y. Huang, "A broadband circularly polarized monopole antenna," *Int. J. RF Microw. Comput. Aided Eng.*, vol. 29, no. 6, pp. 1–8, Dec. 2018.

[15] M. S. Ellis, "Asymmetric circularly polarized open-slot antenna," *Int. J. Microw. Comput. Aided Eng.*, vol. 30, no. 5, pp. 1–10, Jan. 2020.

[16] L. Wang, W. Fang, Y. En, Y. Huang, W. Shao, and B. Yao, "A new broadband circularly polarized square-slot antenna with low axial ratios," *Int. J. Microw. Comput. Aided Eng.*, vol. 29, no. 1, pp. 1–6, Sep. 2018.

[17] M. M. Sharma and R. P. Yadav, "CPW fed ultra-wideband square slot antenna with wideband circular polarization," in *Proc. IEEE Indian Conf. Antennas Propogation (InCAP)*, Dec. 2019, pp. 1–3.

[18] H. Askari, N. Hussain, D. Choi, M. A. Sufian, A. Abbas, and N. Kim, "An AMC-based circularly polarized antenna for 5G sub-6 GHz communications," *Comput., Mater. Continua*, vol. 69, no. 3, pp. 2997–3013, 2021.

[19] Y. Zhang, J. von Hagen, M. Younis, C. Fischer, and W. Wiesbeck, "Planar artificial magnetic conductors and patch antennas," *IEEE Trans. Antennas Propag.*, vol. 51, no. 10, pp. 2704–2712, Oct. 2003.

[20] Q. Chen and H. Zhang, "High-gain circularly polarized Fabry–Pérot patch array antenna with wideband Low-radar-cross-section property," *IEEE Access*, vol. 7, pp. 8885–8889, 2019.

[21] M. E. Hammoumi, N. El Amrani El Idrissi, R. Raad, P. I. Theoharis, F. Tubbal, and S. Abulgasem, "Ultra wideband dual circularly polarized patch antenna for 5G and CubeSat applications," in *Proc. 9th Int. Conf. Wireless Netw. Mobile Commun. (WINCOM)*, Oct. 2022, pp. 1–6.

[22] F. Tubbal, R. Raad, K.-W. Chin, L. Matekovits, B. Butters, and G. Dassano, "A high gain S-band slot antenna with MSS for CubeSat," *Ann. Telecommun.*, vol. 74, nos. 3–4, pp. 223–237, Nov. 2018.

[23] A. Y. Modi, *Metasurface-Based Techniques for Broadband Radar Cross-Section Reduction of Complex Structures*. Tempe, AZ, USA: Arizona State University, 2020.

[24] Z. Xu, J. Tong, T. J. Cui, J. Chang, and D. F. Sievenpiper, "Near-field chiral excitation of universal spin-momentum locking transport of edge waves in microwave metamaterials," *Adv. Photon.*, vol. 4, no. 4, Jul. 2022, Art. no. 046004.

[25] P. I. Theoharis, R. Raad, F. Tubbal, and S. Abulgasem, "High-gain circular polarized microstrip patch array for X-band CubeSat applications," in *Proc. 15th Int. Conf. Signal Process. Commun. Syst. (ICSPCS)*, Dec. 2021, pp. 1–5.

[26] Q. Chen, H. Zhang, L.-C. Yang, B. Xue, and X.-L. Min, "Broadband CPW-fed circularly polarized planar monopole antenna with inverted-L strip and asymmetric ground plane for WLAN application," *Prog. Electromagn. Res. C*, vol. 74, pp. 91–100, 2017.

[27] J.-Y. Jan and C.-Y. Hsiang, "Wideband CPW-fed slot antenna for DCS, PCS, 3G and Bluetooth bands," *Electron. Lett.*, vol. 42, no. 24, pp. 1377–1378, Feb. 2006.

[28] T. S. D. Cheung and J. R. Long, "Shielded passive devices for silicon-based monolithic microwave and millimeter-wave integrated circuits," *IEEE J. Solid-State Circuits*, vol. 41, no. 5, pp. 1183–1200, May 2006.

[29] S.-W. Qu, C. Ruan, and B.-Z. Wang, "Bandwidth enhancement of wide-slot antenna fed by CPW and microstrip line," *IEEE Antennas Wireless Propag. Lett.*, vol. 5, pp. 15–17, 2006.

[30] A. Glisson, "Advanced engineering electromagnetics, by constantine A. Balanis [book review]," *IEEE Antennas Propag. Soc. Newslett.*, vol. 31, no. 6, pp. 24–26, Dec. 1989.

[31] F. Yang and Y. Rahmat-Samii, "Reflection phase characterizations of the EBG ground plane for low profile wire antenna applications," *IEEE Trans. Antennas Propag.*, vol. 51, no. 10, pp. 2691–2703, Oct. 2003.

[32] V. Singh, M. Khalily, and R. Tafazolli, "A metasurface-based electronically steerable compact antenna system with reconfigurable artificial magnetic conductor reflector elements," *Iscience*, vol. 25, no. 12, pp. 1–17, Dec. 2022.

[33] *High Frequency Structure Simulator (HFSS)*. Accessed: Jun. 23, 2023. [Online]. Available: http://www.ansys.com/

[34] *IEEE Standard Test Procedures for Antennas*, Standard ANSI/IEEE Std 149-1979, E. E. A. S. Committee, 1979.

● ● ●